Journal of Materials Chemistry B

Accepted Manuscript

ROYAL SOCIETY OF CHEMISTRY

www.rsc.org/materialsB

Journal Name

RSCPublishing

ARTICLE

In vitro application of Mn-ferrite nanoparticles as novel magnetic hyperthermia agents

Cite this: DOI: 10.1039/x0xx00000x

Received 00th January 2012,
Accepted 00th January 2012

DOI: 10.1039/x0xx00000x

www.rsc.org/

Antonios Makridis,[1] Konstantina Topouridou,[2] Magdalini Tziomaki,[2] Despoina Sakellari,[1] Konstantinos Simeonidis,[1] Mavroeidis Angelakeris,[1] Maria .P. Yavropoulou,[2] John G. Yovos[2] and Orestis Kalogirou[1]

Manganese ferrite nanoparticles were synthesized by a facile, low-cost, environmentally friendly and high yield methodology based on the aqueous co-precipitation of proper salts. Firstly, structural, morphological and magnetic characterization schemes were performed to determine crucial factors for optimizing their heating potential, such as size, polydispersity, saturation magnetization and coercivity. In an effort to simulate the *in vivo* environment of animal tissue phantoms and study the thermal heating effects resulting from Brownian motion and hysteresis losses, nanoparticles at various concentrations were embedded in aqueous media of varying agar concentration. During the *in vitro* application healthy cells (primary bone marrow-derived osteoblasts and 3T3-L1 fibroblast-like preadipocytes) and human osteosarcoma Saos-2 cells, were incubated with manganese ferrite nanoparticles. The heating profile of the particles was studied in different concentrations and in correlation with their potential cytotoxic effect. Our results revealed concentration dependent cytotoxicity profile and uptake efficiency together with variable specific loss power values yet with fast thermal response, opening novel pathways in material selection as hyperthermia agents.

Introduction

Despite the recent advances of biomedical technologies, the therapeutic approach of cancer remains far from desired. Although standard approaches based on surgery, chemotherapy, irradiation, or combinations can significantly improve patient's life expectancy, alternative treatment concepts, such as different hyperthermia types are receiving much of the scientific attention and have already entered into clinical practice.[1] Hyperthermia is also widely used as physical therapy of bone-related diseases, such as inflammatory osteoarticular disorders, malignant bone tumors and bone metastasis.[2,3,4] In whole body hyperthermia where the systemic temperature, by means of a heat bath has to be carefully controlled to, e.g., 41.8◦C, there are different ways of effecting local intracorporal heat generation by means of microwave radiation, by capacitive or inductive coupling of radiofrequency fields, by implanted electrodes, by ultrasound or by lasers. In local hyperthermia, the temperature increases with respect to standard temperature of the human body and is considered to be therapeutically useful over a relatively broad temperature range where different mechanisms of cell damaging occur with increasing temperature. Two treatment modalities are commonly proposed. Treatment at temperature regions of 41–45◦C for up to few hours—actually denoted as hyperthermia—usually combined with other assisting toxic agents, mostly irradiation or chemotherapy, for reliable damage of tumor cells. In contrast, thermoablation aims to the thermal killing of all tumor cells by applying temperatures in excess of at least 50 ◦C in the tumor region for at least few minutes' exposure times. Although these short treatment times and the resulting reliable tumor damage appear promising there are concerns considering critical systemic side effects such as shock syndrome due to sudden release of large amounts of necrotic tumor material and major inflammatory response.[5]

Alternatively, in magnetically mediated hyperthermia, magnetic material is either driven or injected in the tumor, which is then heated by means of an external alternating magnetic field. Despite the application of macroscopic magnetic implants ('seeds'), which are currently in clinical use for special cancer types, recent studies are focused on magnetic nanoparticles as their heat generation potential appears beneficial and they

provide the opportunity of direct tumor targeting.[6] Magnetic nanoparticles (MNPs) being subjected to an AC magnetic field may show remarkable heating effects that are related to losses during the magnetization reversal process of the particles.[7] The temperature enhancement, which occurs in a magnetic nanoparticle system under the influence of an external high frequency magnetic field, can be efficiently used in a wide range of techniques, e.g., hardening of adhesives, in chemistry, e.g., thermosensitive polymers, as well as in biomedicine. In the latter case, cancer therapy based on hyperthermia, drug targeting via thermosensitive magnetic nanoparticles and application of magnetically controllable catheters are important examples.[8] In all cases, it is advantageous to achieve the temperature enhancement needed for a special application with as low as possible dosage of MNPs. Therefore, the quantifiable index of heating efficiency, the specific loss power (SLP), which is measured in watts per gram of magnetic material to be applied, must be high enough.[9,10] This is particularly important for applications where target concentration is very low, for instance in antibody targeting of tumors.[11] Apart from the opportunity of an intense localized heat generation, the application of magnetic nanoparticles offers the possibility of a self-limited temperature rise by using magnetic materials with suitable Curie temperature.[12] When magnetic nanoparticles are incorporated, such treatment modalities are considered as magnetic particle hyperthermia (MPH) with prerequisite the highest possible value of SLP.[13]

Although there is a multitude of known magnetic materials with exploitable heating efficiency, up to date biomedical applicability is strongly restricted by the demand of biocompatibility.[14,15] Thus data scarce regarding the use of alternative systems for MPH[16] while the majority of research is focusing on magnetic iron oxides Fe_3O_4 (magnetite) and γ-Fe_2O_3 (maghemite) which have been proved to be well tolerated by the human body.[17] However, since MPH is continuously gaining power as the least invasive cancer treatment, multifunctional heating-triggered modalities initiating from heating response are currently under intense investigation.[18] In the pursuit of tunable nanomagnetic features, ferrimagnetic or even ferromagnetic particles seem to gain power over typical superparamagnetic ones.[19] Following this scheme, it seems sensible to incorporate other ions such as Co^{2+}, Mn^{2+} and Ni^{2+} into typical ferrites (MFe_2O_4, where M=Co, Mn, Ni...), in an effort to attain tunable magnetic features. Within such an approach, ferrite nanoparticles comprise a promising candidate due to their facile fabrication, chemical stability and their inherently relatively low toxicity,[20] though such systems are still under skepticism for biomedical exploitation.[21,22]

In this work, we propose novel heat mediators with high thermal energy transfer capability. We are currently examining $MnFe_2O_4$ magnetic nanoparticles as potential biomedical heat-triggered carriers.[16] The choice of $MnFe_2O_4$ ferrite nanoparticles is based on their low inherent toxicity, ease of synthesis, physical and chemical stability and tunable magnetic properties together with their suitability as an enhanced MRI contrast agent.[23] Additionally, Mn-ferrites if properly adjusted to the therapeutic temperature can potentially act as smart implants for a self-controlled hyperthermia treatment.[24] Thus the aim of the present study is to investigate how from a system in colloidal form we may test *in vitro* hyperthermia induced by manganese ferrite MNPs on a human osteosarcoma cell line (Saos-2) that possess osteoblastic features.[25] To this end we examined $MnFe_2O_4$ MNPs performance in three different forms, colloidal, phantom-agar based and cellular, in an effort to unravel the connections of physical mechanisms with actual behavior at the cellular level.[26]

Experimental

Nanoparticle Synthesis and Properties

Manganese ferrite nanoparticles were synthesized by the aqueous co-precipitation of $MnSO_4$ and $Fe_2(SO_4)_3$ under strong alkaline conditions and heating. Quantities of $MnSO_4 \cdot xH_2O$ and $Fe_2(SO_4)_3 \cdot xH_2O$ (20 wt% Fe) were dissolved in distilled water to achieve a concentration of 0.05 M each and an Mn-to-Fe molar ratio 1:2. Subsequently, under constant mechanical stirring, the solution temperature rose to 70 °C and was kept at this value throughout the reaction and the aging duration. Nanoparticles were formed as a precipitate after the gradual addition of NaOH solution (50% wt) till the pH reached 11. During this procedure, an intermediate dark red colored precipitate corresponding to the Mn/Fe oxy-hydroxide was rapidly transformed to the black $MnFe_2O_4$ when solution pH became 8. The reaction mixture was gently stirred for one more hour. Finally, the solid product was washed/centrifuged several times with distilled water to achieve an equilibrium conductivity of 500 μS/cm in washing water and dried at 40 °C to receive particles in powder form.

The $MnFe_2O_4$ nanoparticles were characterized by X-ray powder diffraction (XRD), which was carried out in a SIEMENS D500 X-Ray diffractometer using the K_α line of Cu as a radiation source. Particle size and morphology were detected using Transmission Electron Microscopy (TEM), JEOL 2011 operating 200kV. Their magnetic properties were measured by using vibrating sample (VSM – 1.2H/CF/HT Oxford Instruments VSM) and Quantum Design MPMS SQUID magnetometer within a field range of 5 Tesla and a temperature range of 5-300 K.

Heating efficiency of MNPs

To study the impact of colloidal dispersion properties on heating mechanisms, synthesized nanoparticles were dispersed in varying concentration aqueous media, i.e., distilled water together with agarose gel (agar). Agar, a typical polysaccharide, due to its natural origin, low cost and high degree of biocompatibility is employed here as a *phantom* system mimicking cell viscosity (via varying concentration: 0, 1, 5 and 10 wt%) thus as an *in vivo* environment but at the same time as a segregant and a protective material providing colloidal stability. The heating efficiency of the aqueous and phantom

nanoparticle solutions was measured by subjecting the solution to an AC magnetic field at f=765 kHz, at different concentrations varying from 0.25 to 8 mg/mL, and within field amplitudes of 150–300 Oe. The solution was placed in the center of a water cooled induction coil connected to an AC field generator (SPG-10: Ultrahigh Frequency Induction Heating Machine, Shuangping Corporation). In each measurement, heating and cooling sequences were recorded for ample time (≥600s for each sequence). It is important to note that although the value H×f was set at least one order of magnitude above the estimated threshold for major discomfort9 (~5×10^8 A $m^{-1}s^{-1}$), due to the high-frequency choice (clinical trials refer to 100–600 kHz), similar protocols have been currently examined[6,8,11] and may be proven successful in specific cases of smaller diameter body regions by direct injection with much faster times according to the enhanced MNPs heating efficacy as described in the 'Results and Discussion' section. The specific loss power (SLP) of samples was calculated from the following equation.[27]

$$\mathrm{SLP} = \frac{W}{m_m} = \frac{\Delta Q}{\Delta t\, m_m} = C_p \frac{m_f}{m_m} \frac{\Delta T}{\Delta t}$$

which refers to the amount of energy converted into heat (W) per time (Δt) and mass of the magnetic material (m_m) where C_p is the specific heat of the solution ($C_p \sim C_{water}$ = 4.18 J g^{-1} $°C^{-1}$), m_f the solution mass and $\Delta T/\Delta t$ the initial slope of the heating curve in a magnetic field, extracted from experimental data, before the interference of heat conduction becomes crucial.[26]

Cell culture

Saos-2 human osteosarcoma cells (ATCC –HTB-85, LGC Standards, Inc) were cultured in DMEM (Dulbecco's Modified Eagle Medium) nutrient mixture F-12 Ham, supplemented with 1% L-glutamine, 10% of FBS (Fetal Bovine Serum) and 1% Penicillin/Streptomycin at 37 °C and 5% CO_2. The cells were seeded in 6 well plates until 70% confluency and then incubated with the magnetic fluid for 48 hrs. Primary bone marrow-derived osteoblasts and 3T3-L1 fibroblast-like preadipocytes were used as reference healthy cell lines.

Bone marrow from the femoral, tibial, and humeral shafts was flushed from eight-week-old C57BL/6 mouse with AMEM (alpha modification of Eagle's medium) supplemented with 2 mM glutamine, 15% FBS, 100 U/mL penicillin, 100 mg/mL streptomycin, 0.3μg/ml amphotericin B, 50 μg/ml ascorbic acid, 10 mM β-glycerophosphate and 50 ng/ml BMP-2 (bone morphogenetic protein 2). The cells were seeded in 6 well plates and cultured at 37°C and 5% CO_2, with culture medium changes twice a week, for three weeks in order to differentiate into osteoblasts. Control samples were characterized by Alizarin Red staining. After the confirmation of the differentiation by Alizarin Red staining, to avoid assay perturbations, fresh samples of osteoblasts were prepared by incubating with the magnetic fluid for 48 hrs. 3T3-L1 cells were cultured in DMEM supplemented with 2 mM glutamine, 10% FBS, 100 U/mL penicillin and 100 mg/mL streptomycin in 6 well plates at 37°C and 5% CO_2, until 70% confluency. 3T3-L1 cells were then incubated with the magnetic fluid for 48 hrs. After washing with PBS, cells were detached with trypsin-EDTA 5% (3-10 minutes incubation) and transferred to a Neubauer plate. The cytotoxicity was evaluated by Trypan blue method before and after hyperthermia cycles.

***In vitro* treatments with nanoparticles**

To proceed with *in vitro* studies, all three cell lines were incubated with manganese ferrite nanoparticles with optimum structural and magnetic features to comparatively evaluate their *in vitro* hyperthermia performance. Where error bars appear in *in vitro* assay graphs, these correspond to statistical evaluation of four identical samples.

For the cytotoxicity assays three control samples were used: (i) C0a: Control-0a sample: a zero-concentration sample, Saos-2 cells after incubation with sodium deoxycholate, (ii) C0b: Control-0b sample: Saos-2 cells with no treatment, (iii) C1: Control-1 sample: Saos-2 cells with particles, without field application.

For hyperthermia experiments three control samples were used: (iv) water and agar—solvent sample was examined in the preliminary stage where we tested MNPs efficiency, (v) culture medium—to examine the effect of culture medium on hyperthermia, we measured the same quantity of culture medium that underwent similar procedures but without cells or nanoparticles inside (vi) C2: Control-2 sample: Saos-2 cells under field, without particles to check if and how the field solely affects the cells without the presence of MNPs. Analogous control samples were also prepared for the two healthy cell lines.

Cell sample names are coded as SNxx where SN refers to MNPs concentration (S1:0.25 mg/mL or S2:0.5 mg/mL in agreement with solution and agar-solvent samples) and xx is the cell suffix where c (cancer) corresponds to Saos-2 osteoblast, h1 (healthy1) to primary bone marrow-derived osteoblasts and h2 (healthy2) to 3T3-L1 fibroblast-like preadipocytes. During hyperthermia experiment, AC magnetic field remained on until the upper hyperthermia temperature limit of 45°C was achieved. Additionally, during SLP evaluation to calculate the actual heating ability of the nanoparticles, the measurements were corrected using the modified law of cooling.[27,28] Eventually, the MNPs concentration was re-measured at *in vitro* samples after all assays were finished in order to have the final concentration of MNPs adsorbed by the cancer cells.

Cell assays

PRUSSIAN BLUE STAINING

To clarify if nanoparticles are internalized by cells, Prussian blue staining was performed. Analytically, cells after 48hrs incubation with nanoparticles were washed with PBS and fixed with 4% formaldehyde for 15 minutes at room temperature. After washing with water, cells were incubated with a mix of 10% potassium ferrocyanide in water and 20% hydrochloride solution, in 1:1 ratio, for 20 minutes at room temperature. After

washing with water and counterstaining with Nuclear Fast Red staining, optical microscopy followed.

CASPASE 3/7 ASSAY

To investigate if the observed hyperthermia-induced cell viability decrease is attributed to caspase dependent apoptosis, Caspase-Glo®3/7 Assay (Promega, USA) was performed according to manufacturer's instructions. Analytically, 20.000 hyperthermia-treated or control Saos-2 osteoblasts or primary bone marrow-derived osteoblasts in 50μl culture medium were seeded in the proper well of a white-walled 96-well plate. 50μl of Caspase-Glo®3/7 reagent were added to each well and, after a 30 sec gently mix, an one hour incubation at room temperature followed. Luminescence of each sample was measured in a GloMax luminometer and results were expressed in RLU. Background luminescence of blank wells without cells was subtracted from all samples.

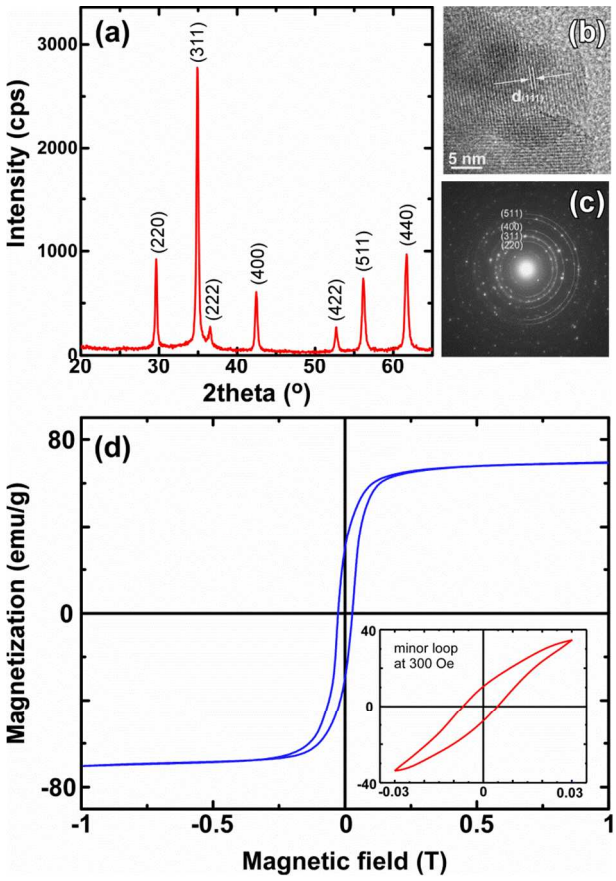

Figure 1: (a) XRD Pattern of manganese ferrite nanoparticles along with (b) TEM image and (c) selected electron diffraction pattern. The main reflections are (220), (311), (222), (400), (422), (511), (440) according to JCPD-PDF #10-0319.(d) Hysteresis loop for the sample recorded at room temperature pointing the ferromagnetic nature of MNPs. Inset shows minor hysteresis loop at maximum hyperthermia field of 300 Oe used for theoretical estimation of hysteresis losses.

Results and Discussion

Nanoparticle features

Figure 1 provides the necessary framework for all subsequent characterization-application schemes as it summarizes the structural and magnetic features of initial magnetic particles under study. Fig. 1a shows the XRD pattern along with transmission electron microscopy (TEM) image (Fig. 1b) and electron diffraction (EDP) pattern (Fig. 1c) for the sample synthesized by co-precipitation as described above. From the XRD diffractogram as compared to PDF #10-0319 the formation of the characteristic spinel structure (S.G.: Fd3m) was confirmed. By measuring the full width at half maximum and using Scherrer's formula, the crystallite size was estimated to be 26 nm. Particle size and crystallinity was also evaluated from TEM analysis. Fig. 1b presents a high resolution TEM image, where crystallographic planes of a single nanoparticle are visible. Estimation of the average diameter of the nanoparticles was performed through statistical analysis of TEM images (not shown) resulted to an average value of 31 nm ± 20% in good agreement with XRD values.

The electron diffraction pattern (Fig. 1c) provides an additional phase verification of manganese ferrites compared with the XRD spectra (Fig. 1a). Fig. 1d depicts the magnetization as a function of the applied magnetic field of the co-precipitate manganese ferrite powder at room temperature. Macroscopically, ferrimagnetic materials behave like ferromagnetic. From now on we will refer in 'ferromagnetic features' in order to describe the macroscopic magnetic behavior of our samples. From the M vs. H curve the ferromagnetic behavior can be deduced by the presence of coercive field and saturation. As revealed from the TEM images nanoparticles seem to have a tendency for agglomeration due to surfactant absence during synthetic procedure, thus of eventual formation of clusters comprising of more than one particles via coupling interactions yielding ferromagnetic features.[27] The saturation magnetization (M_s) for the MNPs is 69.5 emu g^{-1}, comparable to the higher saturation magnetization values reported for manganese ferrite nanoparticles (56-74 emu g^{-1}).[29,30]

The reduced saturation magnetization compared with the corresponding value of the bulk material (110.6 emu g^{-1}) can be attributed to the nanostructure nature of the system and to the size polydispersity resulting to variable magnetic contributions. Inset of Fig. 1d presents the magnetic behavior at the maximum applied AC hyperthermia field used to estimate the hysteresis losses via the energy product (455.32 W/g) of the hysteresis loop.

Heating efficiency

HYPERTHERMIA IN AQUEOUS SOLUTION

To assess the heating efficacy of manganese ferrites in water, magnetic heating characterization is carried out for six samples S1-S6 (with concentrations 0.25, 0.5, 1, 2, 4 and 8 mg/mL, respectively). Fig. 2a,b presents the typical heating efficiency curves of manganese ferrites dispersed in distilled water for all applied magnetic field amplitudes (150 - 300 Oe) for the S1: 0.25 and S2: 0.5 mg/mL concentration samples. In all cases, heating response is tuned by concentration and field amplitude. Except for the 150 Oe sequences where during a measurement

window of 600 s only entrance in hyperthermia region (41–45 °C) was achieved, for the higher field values (≥200 Oe) samples easily surpass hyperthermia threshold. This significant heating response is depicted in Fig. 2c, where SLP, the quantifiable heating efficiency gauge is plotted against concentration for varying field amplitude. The heating signal from the solvent, i.e., the double distilled water was initially measured and used as the control signal in order to selectively isolate only the magnetic heating efficiency of the MNPs themselves, as discussed in previous works of some of us.[27, 28] The 150 Oe sequences are omitted due to their poor performance for clarity reasons.

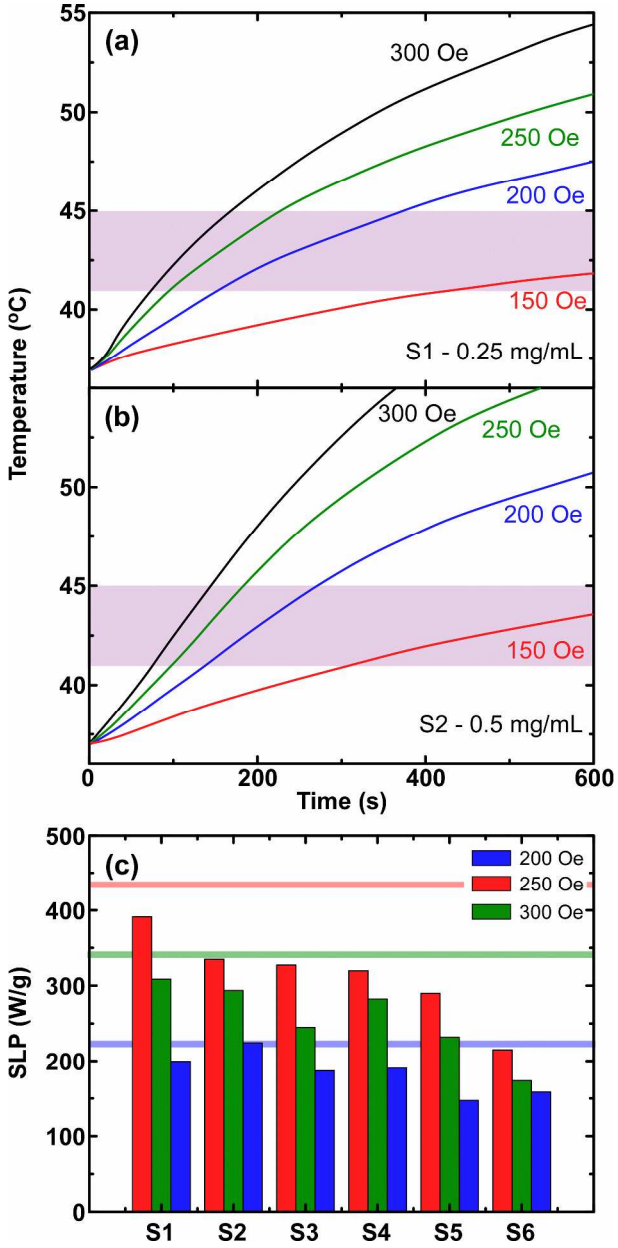

Figure 2: (a) and (b) Typical hyperthermia experimental sequences for the S1: 0.25 and S2: 0.5 mg/mL samples. Shaded band refers to hyperthermia temperature range (41-45 °C). (c) Specific Loss Power (SLP) concentration dependencies at different field amplitude values for S1-S6 samples. The horizontal lines correspond to hysteresis loss values as estimated from minor hysteresis loops recorded at the field amplitudes used in hyperthermia experiments.

The horizontal lines correspond to hysteresis losses estimated by minor hysteresis loops similar to the one shown in inset of Fig. 1d for 300 Oe recorded for powder samples under identical AC hyperthermia field amplitudes. These values correspond to optimum heating efficiency due to hysteresis losses.

However, their estimation via a quasi-static magnetometry sequence is by virtue different that the actual behavior of the MNPs under the high frequency AC hyperthermia field.[31] It seems that for the MNPs under study, the main heating mechanism is connected with hysteresis losses, as expected from the room-temperature ferromagnetism (Fig. 1d).

Although heating efficiency may be further improved if size and morphology issues are accordingly tuned, as far as we know observed SLP values are among the highest ones in relevant studies of ferrite MNPs proposed as alternative hyperthermia agents.[20,26,29]

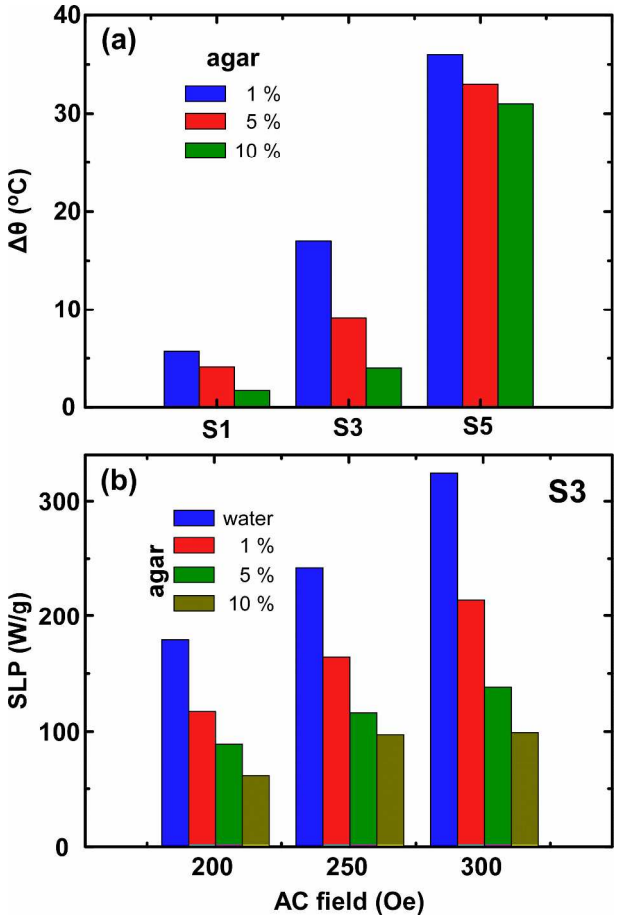

Figure 3: (a) Temperature rise in varying solution concentrations for three representative MNPs concentrations (S1:0.25, S3:1, S5:4 mg/mL). Each column corresponds to different agar weight content (1, 5, 10 wt%) (b) SLP attenuating effect in $MnFe_2O_4$ of Sample S3: 1 mg/mL aqueous suspensions with varying agar concentration ((0; pure water), 1, 5, 10 wt%). All experiments were performed under AC magnetic field frequency of 765 kHz and variable field amplitude as indicated in the x-axis.

HYPERTHERMIA IN PHANTOM SYSTEM

To better understand the inductive heating property of the $MnFe_2O_4$ NPs in a physiological environment, these manganese ferrite samples were dispersed in 1%, 5%, 10% wt% agarose gel, which is used to simulate the *in vivo* environment of animal tissue phantoms.[32]

Agarose matrix resembles cellular environment and provides a flexible option to evaluate how heating response is affected by changing the medium of MNPs from aqueous to a mimicking cellular one. The intracellular nanoparticles generate less heat due to confinement within intracellular vesicles than those dispersed in water. Therefore SLP values will appear suppressed in a physiological environment due to attenuation of the Brownian contribution to heat generation.[33] In an effort to simulate the in vivo environment of animal tissue phantoms in Fig. 3a we present the temperature rise in three characteristic concentrations when agarose gel is incorporated in the colloid. The denser the water solutions in MNPs, the bigger the temperature rise. On the contrary, as the agar solutions become denser under similar MNPs concentration, the temperature rise is suppressed. This effect is readily reflected to SLP values as shown in Fig. 3b, where a representative case of 1 mg/mL MNPs aqueous suspensions with increasing agar concentration (0; pure water), 1, 5, 10 wt%), leading to SLP attenuation 35%, 57%, and 70%, respectively. This effect may be attributed to the fact that agar prevents the Brownian relaxation by freezing the MNPs, in agreement with relevant studies where an SLP value of 53% is decreased in a 5 wt% agarose aqueous colloid.[26] Therefore, free-rotation magnetic nanoparticles may encounter significant SLP decreases in tissue and cellular environments compared to water solution due to remarkably reduced Brownian relaxation loss outlining the need for even higher heating efficiency MNPs.[34]

HYPERTHERMIA IN VITRO

After evaluating the optimum parameters of the MNPs themselves, we continued by performing the cell assay including cytotoxicity and magnetic hyperthermia cycles in Saos-2 osteoblast samples. Sarcoma osteogenic abbreviated as Saos-2, possesses several osteoblastic features and could be useful as a permanent line of human osteoblast-like cells and as a source of bone-related molecules. Some of their advantages include well-documented characterization data, the possibility to obtain large amounts of cells in short time, and the fact that they can be fully differentiated in a manner that the osteoblastic cells naturally do. Therefore, they are incorporated as a valuable model for studying events associated with the osteoblastic differentiation stage in human cells produced by diverse scenario hyperthermia treatments.2[,35,36] For comparison reasons, similar assays were performed in primary bone marrow-derived osteoblasts and 3T3-L1 fibroblast-like preadipocytes selected as healthy reference cell lines. As Fig. 4a depicts healthy cell lines remain practically unaffected from hyperthermia cycles since their viability results remain above 95% of initial control sample. Figs 4b and 4c clearly show that MNPs are eventually internalized by the cells, thus blue color due to MNPs Prussian blue staining is evident in Fig.4c of Sample C1 with respect to control sample C0b (cells only) shown in Fig.4b. These findings are in good agreement with a relevant endocytosis study MNPs were internalized by cancer cells mainly through an energy dependent endocytosis pathway.[37]

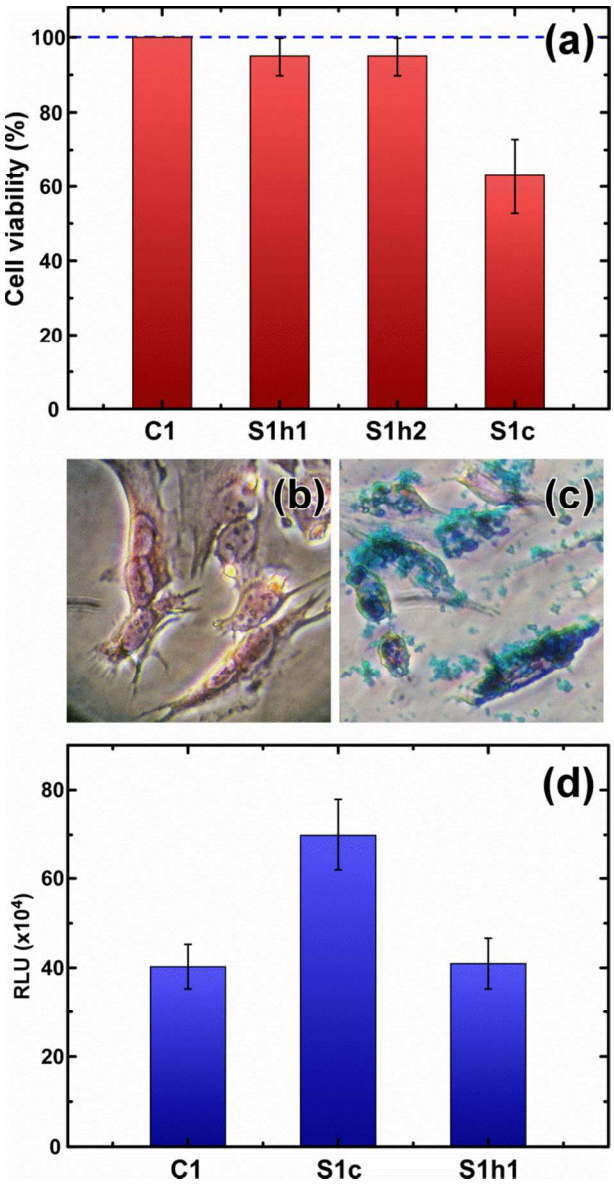

Figure 4: (a): Comparative viability for the three cell lines incubated with 0.25 mg/mL MNPS (S1h1: primary bone marrow-derived osteoblasts, S1h2:3T3-L1 fibroblast-like preadipocytes, S1c: Saos-2 osteoblast) after the first hyperthermia run with respect to control sample C1 (Saos-2 + MNPs). The horizontal blue line refers to initial viabilities (100%) occurring before the hyperthermia runs (b) Optical microscope image (36x) of Saos-2 osteoblast cell line control sample C0b (only Saos-2 cells) and (c) Optical microscope image (36x) of C1 (Saos-2 + MNPs) after Prussian blue staining. (d) Caspase 3/7 activity for hyperthermia-treated samples: Saos-2 osteoblasts (sample S1c) and primary bone marrow-derived osteoblasts (S1h1) together with reference control sample of Saos-2 osteoblasts (C1). Caspase 3/7-dependent apoptosis seems to be induced only in hyperthermia-treated Saos-2 osteoblasts (S1c).

Cell death may be eventually induced by apoptotic mechanisms which may be enhanced either by the longer AC magnetic field

application together with the fact that the hyperthermia run potentially facilitated the cell uptake of MNPs due to the presence of magnetic field.[38]

The occurrence of caspase 3/7-dependent apoptotic mechanism is depicted in Fig. 4d, where a statistically significant increased caspase 3/7 activity was observed only in hyperthermia-treated Saos-2 osteoblasts (sample S1c), in comparison to Saos-2 osteoblasts with MNPs without field (sample C1, p=0.021) and to hyperthermia-treated primary bone marrow-derived osteoblasts (sample S1h1, p=0.031). It seems that the observed hyperthermia-induced cell viability decrease in Saos-2 osteoblasts, as depicted in Fig. 4a (4th column), may be partially attributed to caspase 3/7-dependent apoptosis. Moreover, the non-induced apoptosis in samples C1 and S1h1 seems to be in accordance with the zero-level or very low percentages of cell viability decrease depicted in Fig. 4a (1st and 2nd column, respectively).

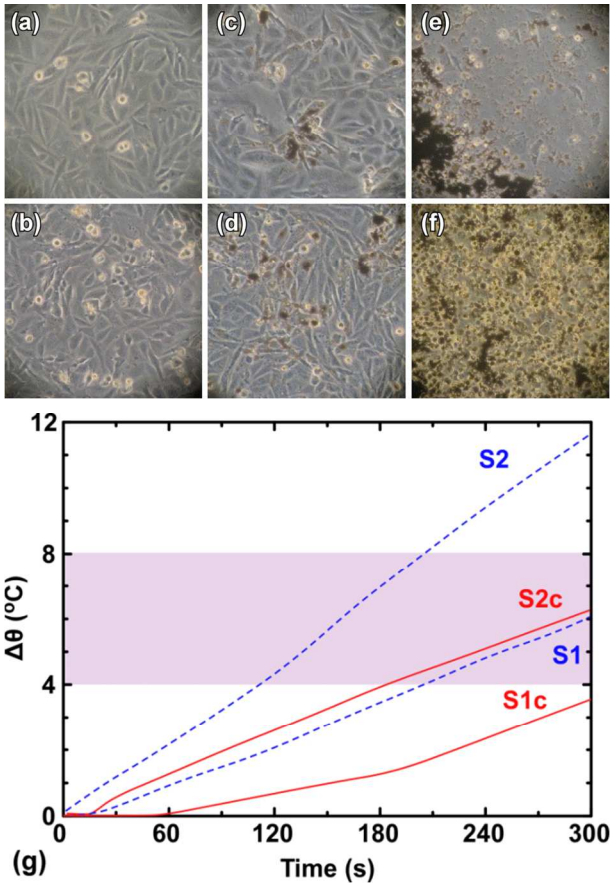

Figure 5: Optical microscope images (40x) of (a) C0b: Saos-2 osteoblast line, (b) C2: Saos-2 osteoblast line after AC field application (c) S1c: Saos-2 osteoblast line after 48 hrs with 0.25 mg/mL MNPs before AC hyperthermia application (d) S2c: Saos-2 osteoblast line after 48 hrs with 0.5 mg/mL MNPs before AC hyperthermia application (e) S1c after hyperthermia (765 kHz, 300 Oe): Saos-2 osteoblast line with 0.25 mg/mL MNPs, (f) S2c after hyperthermia (765 kHz, 300 Oe): Saos-2 osteoblast line with 0.5 mg/mL MNPs. (g): Temperature increase after subtracting all non-magnetic contributions for S1:0.25mg/mL, S2:0.5mg/mL MNPs colloidal solutions. S1c, S2c curves denote cell samples with similar MNPs concentrations. Shaded band refers to hyperthermia region.

Fig. 5 presents an optical qualitative representation of the cytotoxic profile before and after the first hyperthermia session. Cells imaging was performed with optical microscopy. Sodium deoxycholate was used as a biological detergent to lyse cells and to finally have a reference of a zero- cell concentration sample (C0a sample).

In Fig. 5a, C0b sample is shown which comprises of Saos-2 cells while in Fig. 5b C2 sample is depicted which is a similar sample (of cells without MNPs) that was subjected to an AC hyperthermia cycle, to check the sustainability of cells under maximum (300 Oe) AC field application. From direct comparison between the two images, it is unambiguous that the AC hyperthermia fields are very well tolerated by the cancer cells themselves. Fig. 5c and 5d correspond to Saos-2 cells after incubation with Mn-ferrite MNPs and incubation of 48 h and eventual concentrations of 0.25 and 0.5 mg/mL, respectively. Again, the MNPs solely do not seem to significantly harm cell viability. On the contrary, at the right column images (Fig. 5e, 5f) corresponding to imaging after hyperthermia runs, it appears that the cells were shocked and selectively led to loss of viability. Thus, it may be surmised that the AC magnetic field actually seems to facilitate the successful heating effect penetration of MNPs in the cancer cells.

The *in vitro* hyperthermia experiments are summarized in Fig. 5(g). Reference samples S1, S2 (dotted curves) represent the MNPs colloidal solutions of 0.25 mg/mL (bottom curve) and 0.5 mg/mL (top curve) after subtracting all non magnetic heating contributions (i.e., eddy currents, heat exchange with the environment, solvent reference signal). Similarly, curves S1c, S2c (solid ones) correspond to cell samples, where cells were incubated with MNPs for 48 h before AC magnetic hyperthermia experiment. The MNPs concentrations were re-evaluated after the completion of all *in vitro* assays and found to be 0.25 and 0.5 mg/mL, respectively. The heating response of the MNPs is drastically reduced in cellular environment. This effect may be attributed to localization of MNPs within cells that hinders them from fully responding to external magnetic field variations. Moreover, the interaction between MNPs and the local environment adds complexity to the challenge of determining the biological outcome of incorporating nanomaterials.[39]

On the other hand, within the time window of measurement (≤600 s) the desirable temperature levels are achieved, indicated by the shaded band in Fig. 5(g). This becomes more evident in Fig. 6a since the actual heating responses of cell sample S1c (0.25 mg/mL: blue curve) and cell sample S2c (0.5 mg/mL: green curve) are shown for first hyperthermia run (left side of figure) where it is evident that samples remain in effective hyperthermia window (41-45°C) from a value of 235 to 365 s, respectively.

During the *in vitro* experiments, we considered as crucial not to overcome the upper hyperthermia threshold of 45°C in order not to harmfully shock surrounding environment (normal tissue or cells in assays of possible *in vivo* samples) so measurement time sequence ended when approaching at this temperature limit. The right part of Fig. 6a corresponds to the second

hyperthermia run occurring practically after two days interval, where cell samples were again incubated and provided with the proper conditions to continue growing. As it can been seen, this time the response under AC magnetic field is milder, yielding much higher time intervals (18-23 minutes) in the hyperthermia region, an effect probably associated with the actual amount of MNPs internalized by the cancer cells. Optical microscopy together with cell viability assays were performed in all intermediate stages in order to qualitatively as well as quantitatively evaluate the cell damage induced by temperature increase due to magnetic hyperthermia.

In bar diagram of Fig. 6b the cell viability results obtained by Trypan Blue exclusion test are presented for the first and the second hyperthermia run. To begin with, C2 control sample is a cell sample undergone hyperthermia treatment (AC field application) but with 0% MNPs concentration. This result is in agreement with the findings of Figs. 5a, 5b showing that solely the magnetic field without MNPs has not a cytotoxic effect in cancer cells.

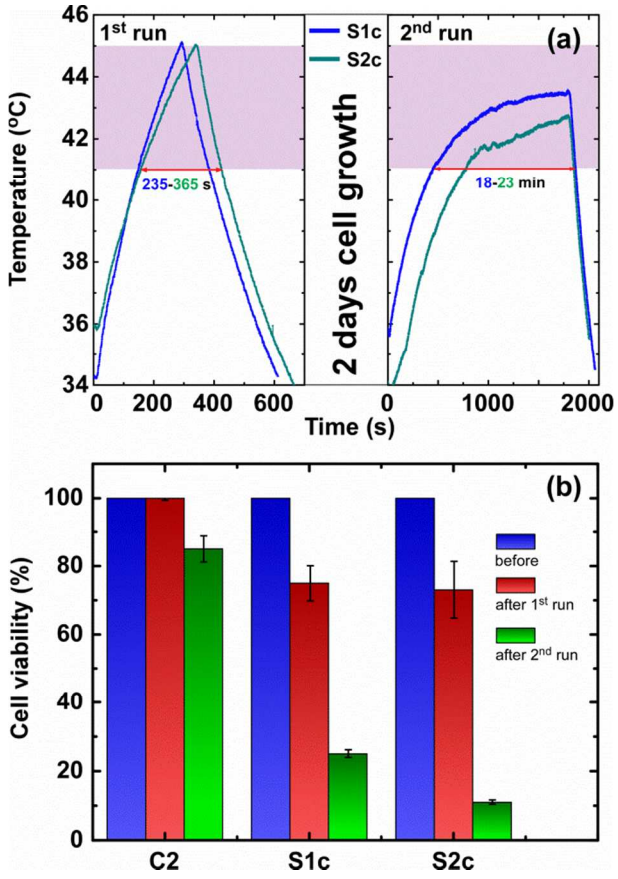

Figure 6: (a) 2 cycle hyperthermia experiments for samples S1c (blue curve) and sample S2c (green curve). Shaded band denotes hyperthermia temperature region. Between two hyperthermia runs a two days cell growth stage took place. (b) Cell viability assays before and after 1st hyperthermia and 2nd hyperthermia runs. C2 refers to hyperthermia control sample: Saos-2 cells without MNPs only subjected to AC magnetic field of 765 kHz, 300 Oe, while S1c and S2c correspond to Saos-2 osteoblast samples with 0.25 mg/mL and 0.5 mg/mL, respectively.

From Fig. 6b it is also apparent that after the first run, for samples incubated with MNPs, hyperthermia manages to partially reduce the viability of cancer cells (only ~ 20% of cell viability reduction, yet of statistical significance since p=0.003 and p=0.014 for S1c and S2c samples respectively, in comparison to C2 control sample after first hyperthermia run). It seems that the limited time duration of the first hyperthermia run (≤365 s) is the actual reason for the limited toxicity effect. This was the actual reason for re-subjecting the sample in a second hyperthermia run after a two days intermission, where cells were left to relax and regain under appropriate harvesting conditions. Fig. 6b also represents the cell viability behavior after second hyperthermia run, where it is apparent that now hyperthermia successfully manages to reduce the viability up to 90% (for sample S2c with 0.5 mg/mL MNPs, p=0.003 in comparison to C2 control sample after second run). A substantial and statistically significant reduction in cell viability after second hyperthermia run is also observed for sample S1c with 0.25 mg/mL MNPs (p=0.002 in comparison to C2 control sample after second run). Again, control sample (C2) maintained high viability values (over 90%).

Thus, hyperthermia treatment may act synergistically as cellular-level cancer therapy since the use of applied magnetic fields may activate naive T cell populations which were otherwise poorly responsive to stimulation.[40] Since naive T cells are more effective for cancer subtypes increasing the yield and activity of antigen-specific T cells expanded from naive precursors. Recently, another interesting effect of hyperthermia treatment is the potential activation of heat-shock proteins (HSPs).2,[41,42] These are a group of proteins, usually called stress proteins, existing in all of the living creatures covering bacteria to human beings and have been recently considered to be a new powerful cancer immunotherapy scheme.[43] They can be induced in living cells by hyperthermia among other causes such as metabolic stress and oxygen deprivation. It has been shown that HSPs are expressed in human osteosarcomas. The inducible Hsp70 only expressed in response to stress is a useful biomarker, since it has critical functions during cell growth, specifically associated with the cell cycle and proliferative response. The role of HSP expression levels and its antiapoptotic effects against caspase activation is an issue under study and needs to be elucidated in future.

Conclusions

$MnFe_2O_4$ nanoparticles, synthesized by a eco-friendly, facile, high-yield, scalable methodology are shown to be promising candidates for hyperthermia purposes since they present a moderate magnetization, chemical stability and high specific loss power together with low inherent toxicity even with the absence of surfactants. Prior to *in vitro* hyperthermia testing, phantom systems based on varying agar-concentration demonstrated the effect of MNPs immobilization within the cellular entity. Sole AC magnetic field application had no influence on cell viability, yet in combination with Mn-ferrite MNPs is rather harmful to Saos-2 as a hyperthermia heating

agent scheme while healthy cell lines (primary bone marrow-derived osteoblasts, 3T3-L1 fibroblast-like preadipocytes) seem to tolerate fairly well this treatment. By employment of two subsequent hyperthermia cycles, the cytotoxicity effect on Saos-2 osteoblasts is maximized. Finally, magnetic particle hyperthermia may be widely proposed as multifold physical therapy provoking a series of heat shocks either directly or indirectly with a pronounced inhibitory effect selectively on human osteosarcoma cells.

Notes and references

a Department of Physics, Faculty of Sciences, Aristotle University of Thessaloniki, 54124 Thessaloniki, Greece
b Division of Molecular Endocrinology, AHEPA University Hospital, Aristotle University of Thessaloniki, 54124 Thessaloniki, Greece

References

1 A. P. Khandhar, R. M. Ferguson, J. A. Simon, and K. M. Krishnan, *J. Appl. Phys.,* 2012, **111**, 7 07B306–07B306-3.
2 K. Trieb, H. Blahovec and B. Kubista, *Cell Biochem Funct.,* 2007, **25**, 669–672.
3 M. Alcaide, C. Ramírez-Santillán, M. José Feito, M. Matesanz, E. Ruiz-Hernández, D. Arcos, M. Vallet-Regí, and M. Teresa Portolés, *J. Biomed. Mater. Res. Part A.*, 2012, **100**(1), 64-71.
4 F.M. Martín-Saavedra, E. Ruíz-Hernández, A. Boré, D. Arcos, M. Vallet-Regí and N. Vilaboa, *Acta Biomaterialia.*, 2010, **6**, 4522–4531.
5 P. Moroz, S.K. Jones and B. N. Gray, *Int. J. Hyperthermia.*, 2002, **18**(4), 267-84.
6 B. Kozissnik, A. C. Bohorquez, J. Dobson and C. Rinaldi, *Int. J. Hyperthermia.*, 2013, **29**(8) 706–714.
7 K. Krishnan, *IEEE Trans Magn.*, 2010, **46**, 2523.
8 Q.A. Pankhurst, N.K.T. Thanh, S.K. Jones and J. Dobson, *J. Phys. D*, 2009, **42**, 224001.
9 R. Hergt, S. Dutz, R. Müller and M. Zeisberger, *J. Phys.: Condens. Matter*, 2006, **18**, S2919.
10 S. Dutz and R. Hergt, *Int. J. Hyperthermia.*, 2013, **29**(8), 790–800.
11 S.E. Barry, *Int. J. Hyperthermia.*, 2008, **24**, 451–466.
12 A. T. Apostolov, I. N. Apostolova and J. M. Wesselinowa, *J. Appl. Phys.*, 2011, **109**, 083939.
13 K. D. Bakoglidis, K. Simeonidis, D. Sakellari, G. Stefanou and M. Angelakeris, *IEEE Trans. Magn.*, 2012, **48**(4), 1320.
14 A. K. Gupta and S. Wells, *IEEE Transactions on NanoBioscience.*, 2004, **3**(1), 66-73.
15 L. H. Reddy, J. L. Arias, J. Nicolas and P. Couvreur, *Chem. Rev.*, 2012, **112**, 5818–5878.
16 D. Yoo, J.-H. Lee, T.-H. Shin and J. Cheon, *Accounts of Chemical Research.*, **44**, 863.
17 S. Laurent, S. Dutz, U. O. Häfeli and M. Mahmoudi, *Advances in Colloid and Interface Science.*, 2011, **166**, 8–23.
18 I. Hilger, *Int. J. Hyperthermia.*, 2013, **29**(8), 828–834.
19 C. Martinez-Boubeta, K. Simeonidis, David Serantes, I. Conde-Leborán, I. Kazakis, G. Stefanou, L. Peňa, R. Galceran, Ll. Balcells, C. Monty, D. Baldomir, M. Mitrakas, and M. Angelakeris, 2012, *Adv. Func. Mater.*, **22**, 3737–3744.
20 I. Sharifi, H. Shokrollahi and S. Amiri, *J. Magn. Magn. Mater.*, 2012, **324** , 903–915.
21 E.L. Verde, G. T. Landi, M. S. Carrião, A. L. Drummond, J. A. Gomes, E. D. Vieira, M. H. Sousa, and A. F. Bakuzis, *AIP Advances.*, **2**, 2012, 032120.
22 A. Tomitaka, H. Kobayashi, T. Yamada, M. Jeun, S. Bae, and Y. Takemura, *Journal of Physics: Conference Series.*, 2010, **200** 122010.
23 K. Vamvakidis, D. Sakellari, M. Angelakeris and C. Dendrinou-Samara, *J. Nanopart. Res.*, 2013, **15**, 1743.
24 M. Reza Barati, K. Suzuki, C. Selomulya and J. S. Garitaonandia, *IEEE Trans Magn.*, 2013, **49**(7), 3460-3463.
25 S. B. Rodan, Y. Imai, M. A. Thiede, G Wesolowski, D. Thompson, Z. Bar-Shavit, S. Shull, K. Mann and G. A. Rodan, *Cancer Res.*, 1987, **47**, 4961-4966.
26 X. Li Liu, E. S. G. Choo, A. S. Ahmed, L. Y. Zhao, Y. Yang, R. V. Ramanujan, J. M. Xue, D. D. Fan, H. M. Fan and J. Ding, *J. Mater. Chem. B*, 2014, **2**, 120.
27 K. Simeonidis, C. Martinez-Boubeta, Ll. Balcells, C. Monty, G. Stavropoulos, M. Mitrakas, A. Matsakidou, G. Vourlias, and M. Angelakeris, *J. Appl. Phys.*, 2013, **114**(10), 103904.
28 A. Chalkidou, K. Simeonidis , M. Angelakeris, T. Samaras, C. Martinez-Boubeta, Ll. Balcells, K. Papazisis, C. Dendrinou-Samara and O. Kalogirou, *J. Magn. Magn. Mater.*, 2011, **323**, 775–780.
29 A. Doaga, A.M. Cojocariu, W. Amin, F. Heib, P. Bender, R. Hempelmann and O.F. Caltun, *Materials Chemistry and Physics*, 2013, **143**(1), 305-310.
30 A. S. Nikolic, M. Boskovic, V. Spasojevic, B. Jancar, B. Antic, *Materials Letters*, 2014, **120**, 86-89.
31 C. L. Dennis and R. Ivkov, 2013, *Int. J. Hyperthermia.*, 2013, **29**(8) 715–729.
32 M. Salloum, R. H. Ma, D. Weeks and L. Zhu, *Int. J. Hyperthermia.*, 2008, **24**(4), 337–345.
33 J. P. Fortin, F. Gazeau and C. Wilhelm, *European Biophysics Journal.*, 2008, **37**(2), 223–228.
34 A. P. Khandhar, R. M. Ferguson and K. M. Krishnan, *J. Appl. Phys.*, 2011, **109**, 7B310-7B3103.
35 A. Baeza, D. Arcos and M. Vallet-Regí, *J. Phys.: Condens. Matter.*, 2013, **25**, 484003.
36 M. Vila, M. C. Matesanz, G. Gonçalves, M. J. Feito, J. Linares, P. A. A. P. Marques, M. T. Portolés and M. Vallet Regi, *Nanotechnology.*, 2014, **25**, 035101.
37 Q. Liu, J. Zhang, W. Xia and H. Gu, *Nanoscale.*, 2012, **4**, 3415-3421.
38 L. K. Bogart, A. Taylor, Y. Cesbron, P. Murray and R. Lévy, *ACS Nano.*, 2012, **6**, 5961-5971.
39 M. Xu, J. Li, H. Iwai, Q. Mei, D. Fujita, H. Su, H. Chen and N. Hanagata, *Scientific Reports.*, 2012, **2**, 406.
40 K. Perica, A. Tu, A. Richter, J. Glick Bieler, M. Edidin and J. P. Schneck, *ACS Nano.*, 2014, **8**, 2252-60.
41 A. Ito, F. Matsuoka, H. Honda and T. Kobayashi, *Cancer gene ther.*, 2003, **10**(12), 918-925.

42 V. L. Vega, W. Charles and A. De Maio, *Cell Stress and Chaperones*, 2012, **15**(5), 517-527.
43 M. Jeun, J. W. Jeoung, S. Moon, Y. J. Kim, S. Lee, S. H. Paek, K. W. Chung, K. H. Park and S. Bae, *Biomaterials*., 2011, **32**, 387-394.

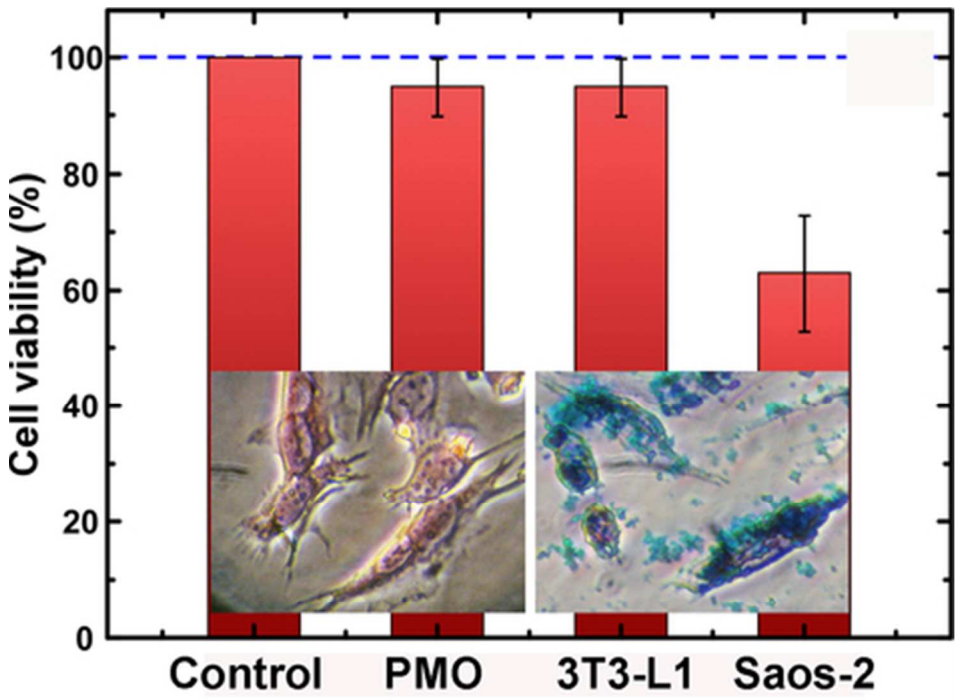

A hyperthermia heating agent of Mn-ferrite MNPs is selectively harmful for Saos-2 osteoblasts.
39x29mm (300 x 300 DPI)